Journal of Engineering Mathematics **43:** 153–171, 2002.

Flow of architectural coatings on complex surfaces; theory and experiment

L.W. SCHWARTZ*,[1] and R.R. ELEY[2]
[1]*Departments of Mechanical Engineering and Mathematical Sciences, University of Delaware, Newark, DE 19716, USA; *Author for correspondence*
[2]*ICI Paints Research Center, Strongsville, OH 44136, USA*

Received 2 August 2001; accepted in revised form 6 May 2002

Abstract. A mathematical model is developed to predict the three-dimensional time-dependent flow of a non-Newtonian shear-thinning liquid coating on a non-planar substrate. The model employs the lubrication approximation and other simplifications. Results are compared with experimental observation of the drainage flow out of an axisymmetric indentation in a vertical substrate. A straightforward experimental method is developed to capture quantitative measurements of the evolving free-surface shapes. Two different architectural paints are used. The agreement between theory and experiment is good overall; however, agreement is better for one of the paints, presumably due to inadequate rheological modeling of the other. Improved understanding of the coating flow of these liquids can be expected to lead to improved products and processes.

Key words: complex substrate shape, experimental validation, industrial coating, lubrication approximation

1. Introduction

In terms of value added, the coating industry is of very significant size. Virtually all manufactured products require coating, for both decorative and protective reasons. Because the industry is fragmented, it is difficult to assign to it a precise yearly value, but it is surely several hundred billion dollars worldwide. For example, the coating of new automobiles and trucks is at least a thirty-billion-dollar yearly activity. Considering the size of the industry, it is perhaps surprising therefore that large-scale numerical modeling of coating flow is in its relative infancy.

Most commonly, coatings are applied as liquids; these liquids continue to flow until the coating is fully dry. Thus fluid-mechanics modeling is potentially of great benefit in helping to improve the flow performance of candidate coatings. Mathematical modeling, employing the low-speed, small-surface-slope approximation, referred to commonly as the *lubrication approximation*, has been in use for many years. Early work included the prediction of coating thickness on plates withdrawn from a liquid bath, an explanation for rib-defect formation in blade or rotary coating, and the calculation of the leveling effect of surface tension for a slightly nonuniform liquid surface [1–3]. For the most part, lubrication-theory analysis has been restricted to Newtonian liquids; however, Tallmadge extended the plate-withdrawal theory to power-law liquids [4]. More recently, two-dimensional lubrication flow, using a three-constant Ellis rheological model, where the viscosity at any point within the coating is a particular function of the shear rate-of-strain, was used in a study of contact-line motion [5].

The above analyses assumed that the flow field is two-dimensional. Only recently have fully three-dimensional unsteady flows been calculated. Perhaps the earliest work was our simulation of drainage, under gravity, of a small droplet on a vertical wall [6]. Although a coarse mesh was used, the calculated sequence of droplet shapes was quite similar to the experimental results of Tanner [7]. Continual increases in computer power have allowed more complex flows to be calculated. As the mesh size becomes smaller, in finite-difference calculations, it also becomes necessary to use partially-implicit methods in order to maintain numerical stability. We have calculated drop break-up on heterogeneous substrates; that is substrates that exhibit a pattern of different values of equilibrium contact angle [8, 9]. Spontaneous dewetting, as is commonly seen when water 'beads up' on a freshly-waxed car, has been simulated and appears to be in good agreement with observation [10, 11]. These simulations use a type of alternating-direction implicit (ADI) algorithm. The ADI technique was originally conceived by Peaceman and co-workers [12]. Three-dimensional drainage calculations, including both gravity and applied surface stresses have recently been reported by Eres *et al.* [13]. For small deviations from a steadily propagating two-dimensional solution, the numerical solution faithfully reproduces the results of linear stability analyses for either driving mechanism [14, 15]. Other recent three-dimensional-simulation results can be found in the work of Lopez *et al.* who consider the stability and evolution of a dry spot in a liquid coating layer [16].

In this paper we treat a particular industrially-motivated problem. We consider a vertical substrate to which a thin uniform liquid coating has been applied. There is an axisymmetric indentation in the substrate whose dimensions are approximately 7 mm in diameter and 1 mm in depth. This flat-bottomed indentation has sloping side walls. The trapezoidal cross section of the indentation is shown in Figure 6. In light frame construction of residential dwellings in North America, doorways and windows are encased with machined wooden pieces. These casings are usually fastened with a nail gun. The nail head is set below the surface of the wood. Unless the resulting indentations are laboriously filled with putty which is then allowed to dry and harden, subsequent painting of vertical casing elements will likely result in the unsightly drip marks that are considered here. Development of architectural paints whose flow properties have been adjusted, so as to minimize the labor involved in their application, is a principal research goal of the industry.

The next section outlines the theoretical basis for the computer simulation. The model requires the specification of fluid and geometric parameters and will accept an arbitrary, experimentally-measured, data set giving viscosity as a function of applied shear stress. The experimental technique for generating the dripmarks, capturing their images in real time, and measuring their surface profiles is given in Section 3. Sections through the liquid are taken from the photographic flow record, although a number of corrections need to be applied. Direct comparison between theory and experimental flow results can be found in Section 4 for two different paints. This section also contains theoretical predictions showing how the present shear-thinning flow differs from the flow expected for a Newtonian liquid. The effect on the drainage profile of indentation diameter is also considered. Additional perspective on this work and plans for future investigation may be found in the concluding section.

2. The theoretical model

For slow flow of thin layers of Newtonian liquid, the lubrication approximation has a well-established mathematical foundation. It is the leading-order approximation that results when

the flow-inclination angle, relative to the substrate, is considered to be a small parameter [17–19]. We use a right-handed three-dimensional Cartesian coordinate system with the (x, y) plane lying on the flat or 'land' area of the substrate. The substrate is oriented vertically with the x-axis directed downward while the y-axis is horizontal; z is distance measured perpendicular to the substrate. At any instant of time, the free surface of the coating is given by the function $z = h(x, y, t)$ where t is time. The liquid layer is bounded above by a tractionless free boundary upon which surface tension acts. The layer is bounded below by the substrate whose equation is $z = h_1(x, y)$. Thus, the thickness of the coating is given by $h - h_1$. Here h_1 is taken to be the equation of a circular indentation with a flat bottom, corresponding, for example, to a nail head that has been 'set' below the level of the substrate using a nailpunch.

The evolution equation for the free-surface shape follows from application of the global mass-conservation equation

$$\frac{\partial h}{\partial t} = -\nabla \cdot \mathbf{Q} \,. \tag{1}$$

Here ∇ is the two-dimensional differential operator with respect to the orthogonal substrate coordinates x and y. $\mathbf{Q}$ is the flux vector defined by

$$\mathbf{Q} = \int_{h_1}^{h} \mathbf{u} \, \mathrm{d}z,$$

where $\mathbf{u}$ is the vector velocity; $\mathbf{u}$ is essentially parallel to the flat substrate. For fully-developed flow in a two-dimensional channel of depth h, the relationship between $\mathbf{Q}$ and the driving pressure gradient is

$$\mathbf{Q} = -\frac{h^3}{3\mu} \nabla p \,, \tag{2}$$

which is simply Poiseuille's law for a Newtonian liquid of constant viscosity μ. This law will now be modified to account for shear-thinning behavior.

We will assume that the coating liquid falls into the class referred to as 'generalized Newtonian' so that the viscosity μ depends only on the local value of shear stress. (See Bird *et al.* [20, pp. 205–256].) It is usual practice to assume a simple functional relation between μ and the shear stress τ with one or more adjustable parameters. For example, the so-called Ellis model is one possible choice. According to this often-used model, the relation is

$$\frac{1}{\mu} = \frac{1}{\mu_*} \left(1 + \left| \frac{\tau}{\tau_{1/2}} \right|^{\alpha - 1} \right). \tag{3}$$

Here μ_* is the viscosity when the stress is zero. The input parameter $\tau_{1/2}$ is the value of shear stress for which the viscosity has been reduced by a factor of one-half. Shear-thinning behavior is also controlled by the input exponent α; $\alpha = 1$ corresponds to Newtonian flow and $\alpha > 1$ is the range for shear-thinning behavior.

It is now necessary to find the flux Q in the generalized Newtonian case. We apply the no-slip condition on the substrate and the condition $\tau = 0$ on $z = h$. In scalar form, the constitutive law is simply

$$\tau = \mu(\tau) \frac{\partial u}{\partial z},$$

which can be integrated to find the velocity profile across the thin liquid layer. The key to this integration is the recognition that the shear stress τ is a linear function of the normal coordinate z. Further details are given in the Appendix. A method is developed there that enables the direct use of experimental data for $\mu(\tau)$ without the need to fit these data to an Ellis, or any other, model. The general result for the flux is

$$\mathbf{Q} = -\frac{\nabla p}{3\mu_*}\,(h-h_1)^3\;F, \tag{4}$$

where the 'fluidity magnification factor' F represents the fractional increase in flow due to shear thinning. It depends on local values of the pressure-gradient magnitude and the total liquid depth $h - h_1$. For example, had the Ellis model been used, we would have had

$$F = \left[1 + \left(\frac{3}{\alpha+2}\right)\left(\frac{|\,\nabla p\,|\,(h-h_1)}{\tau_{1/2}}\right)^{\alpha-1}\right].$$

Note that, when the Ellis reference stress $\tau_{1/2}$ is very large, the additional flow due to shear thinning, as given by the second term in the bracketed expression, is quite small.

For the present drainage problem, the pressure has contributions from the capillary pressure, which is essentially the product of the surface curvature and the surface tension, and from gravity. Gravity is taken to act in the downward or positive x-direction. The unit vector in the x-direction is $\mathbf{i}$. Thus

$$\nabla p = -\sigma\nabla\nabla^2 h - \rho g\mathbf{i}, \tag{5}$$

where σ is surface tension, ρ is density and g is the acceleration of gravity. For small surface inclination, $\nabla^2 h$ is approximately equal to the surface curvature. A model for gravity drainage flow in one space dimension, using the Ellis model, was reported by Weidner and Schwartz [5]. Kim *et al.* [21] modeled flow of a Newtonian coating on a roughened substrate simply by using the local total flow depth $h - h_1$, to replace h in (2), just as we are doing here. This is similar to the method employed by Kalliadasis and Homsy who consider the stability of flow over substrate topography [22]. Three-dimensional flow on a surface containing gravure cells, as used in printing operations, was simulated by Schwartz *et al.* [23]. In that work the gravure indentations were modeled using the total depth $h - h_1$ and Ellis rheology was also used.

The Ellis model is a typical generalized Newtonian-flow law; sometimes other laws provide a better fit to the experimental data [20]. No single functional form is ever a good model for all coatings. Here, instead, we use the procedure described in the Appendix that allows tabular data for $\mu(\tau)$ to be used directly. This eliminates a source of error and also simplifies the reduction of experimental results since there is no need to fit the data to a particular *a priori* model.

It is useful, for computation, to write the evolution equation in dimensionless variables. The equation becomes

$$\frac{\partial h}{\partial t} = -\frac{\partial s}{\partial x} - \nabla\cdot(s\nabla\nabla^2 h)\;. \tag{6}$$

Here s is the 'permeability', taking into account the thinning behavior. Specifically

$$s = (h-h_1)^3 F, \tag{7}$$

where F is again the dimensionless factor in square brackets in Equation (4) as determined from the rheological data, or 'flow curve', using the method given in the Appendix. In (6) and (7), the thicknesses are written as multiples of h_0, the initial uniform coating thickness on the flat or 'land' part of the substrate. Thus h_0 is the unit of length in the z-direction. For the substrate coordinates (x, y), the length unit is

$$L_1 = \left(\frac{\sigma h_0}{\rho g}\right)^{1/3} \quad . \tag{8a}$$

The reference time is

$$T_1^* = \frac{3\mu_0 L_1}{\rho g h_0^2}, \tag{8b}$$

where the reference viscosity is $\mu_0 = \mu(\tau_0)$ and $\tau_0 = \rho g h_0$, the substrate shear stress for gravity drainage of the initial uniform coating of thickness h_0. Once the configuration of the initial coating is specified, Equation (6) is used to predict its subsequent flow behavior. Note that the dimensional scaling results in an evolution equation that is free of parameters.

The dimensionless equation (6) is solved by a finite-difference method in space and time. The substrate is discretized into an $M \times N$ rectangular computational domain. Spatial derivatives are approximated using central differences; thus the method is second-order accurate in space. Time marching is made efficient using a novel semi-implicit method. It is similar, in principle, to alternating-direction (ADI) methods used for second-order diffusive problems, as discussed by Peaceman [12]. Nonlinear pre-factors in s are evaluated at the 'old' time level. Thus, the method is only first-order accurate in time. However convergence is easily verified under temporal refinement and time-steps are adjusted accordingly. In general, the spatial differential operators are split into x and y parts. The h values are updated implicitly, but sequentially, leading to pentadiagonal banded systems since the evolution equation (6) is fourth-order in space. These banded linear systems are solved efficiently by Gauss elimination. Odd-order normal derivatives are taken to be zero on the edges of the computational window. Thus the computational window must extend at least several radii upstream and downstream of the indentation. All computational results presented here have been verified as being converged to graphical accuracy. A point-spacing $\Delta x = 0{\cdot}05R$, where R is the radius of the indentation at the land level, is sufficient to achieve this accuracy in all cases.

It can easily be shown that an explicit, *i.e.* simple Euler, time integration is unstable for this spatially fourth-order system unless

$$\Delta t < O(\Delta x)^4 \, . \tag{9}$$

Here Δt is the time step, Δx is the space step, and O signifies mathematical order of magnitude. Because of this constraint, the present method is faster by several orders of magnitude compared to an explicit scheme. The method is also much faster than an implicit time integration were the ADI technique not used, in which case very large sparse systems of equations would have had to be solved. Using the ADI scheme, the computer time is proportional to the number MN of calculated h values. Typical calculations use about 20,000 surface ordinates and require less than one minute on a PC with an Athlon 1·2 gHz processor. The numerical algorithm is written in Fortran and the public-domain Linux operating system is used. Rendered output displays employ the Geomview public-domain graphics package (*viz.* http://www.geomview.org). We note that the theoretical problem is bilaterally symmetric

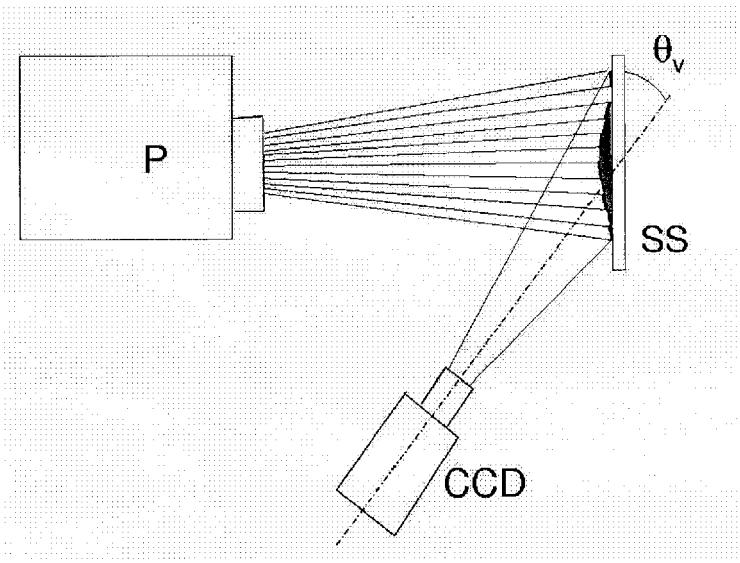

Figure 1. Schematic experimental set-up, top view. The projector P places equally-spaced black vertical lines on the surface of the liquid coating, shown shaded. The camera CCD is inclined at an angle θ_v to the substrate SS. For the results reported here the camera angle θ_v is 46·1°.

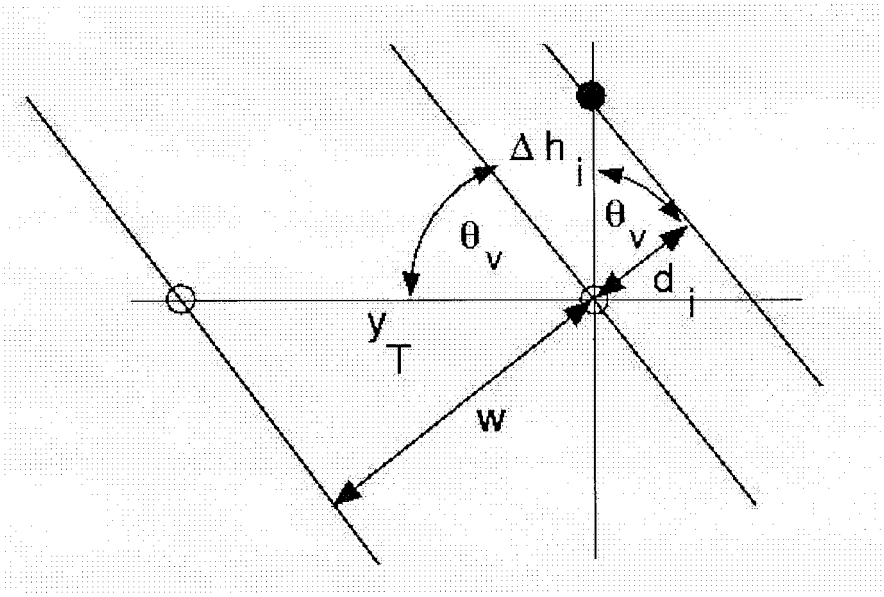

Figure 2. Grid is projected from above. Camera is inclined at angle θ_V. Actual ruling spacing is y_T. Camera picture spacing is w if the surface is flat. Here the right-most open point is displaced upward an amount Δh_i to the black point. The camera picture shows that the apparent point spacing has been increased from w to $w + d_i$. Each d_i may be positive or negative.

about the vertical centerline. This symmetry is exploited in the simulation and reduces the computational load by a factor of one-half.

3. Experimental procedure

Two different paints were applied to an aluminum substrate in which a precision-drilled flat-bottomed indentation had been made. The same substrate was used for both paints and it was carefully cleaned between tests. The indentation has a radius R of 0·357 cm at the land level and a depth of 0·102 cm. This axisymmetric indentation has a flat bottom and side walls with a 45 degree slope. The substrate was held in a vertical orientation, so that the paint flows out of the indentation due to gravity. Initially the paint surface was flat; the paint was applied by means of a precision instrument known as a drawdown bar. The initial thickness was $h_0 =$ 0·022 cm for all experiments reported here. The two paints were an interior flat latex that will be called Paint IL and an exterior flat latex called Paint 22. The values of surface tension and density for the two paints were similar. The measured values were $\sigma = 36{\cdot}5$ dynes/cm, $\rho = 1{\cdot}34$ gm/cm^3 for Paint 22 and $\sigma = 35{\cdot}6$ dynes/cm, $\rho = 1{\cdot}38$ gm/cm^3 for Paint IL. A TA Instruments AR-1000N Controlled Stress Rheometer was used to measure viscosity for the two paints as a function of shear stress. Results for the two paints are given in the next section.

The image of the paint free surface was recorded photographically, as a function of time, with a CCD camera and a video capture card. The evolving free-surface shapes were then compared with results of the theoretical and numerical model described above. The experimental set-up is shown schematically in Figure 1. A projector P projects a set of equally-spaced, nominally vertical, lines onto the paint-covered substrate. The projector is perpendicular to the substrate. Unless the CCD camera is also held at right angles to the substrate, the projected vertical lines will be distorted because the liquid surface is nonuniform. The shape of any distorted vertical line is actually a scaled vertical cross section of the free surface. Good results were obtained when the camera was set at about a 45 degree angle to the substrate. This angle is denoted as θ_V in the figure.

In Figure 2 the true spacing between lines projected onto a vertical plane is y_T. The projected lines viewed in-plane are represented as open circles in the figure. When viewed at an angle $\theta_v < 90°$, the apparent line spacing will be w for a planar surface, where $w < Y_T$. Suppose, however, the surface has a local variation in height, so that the ordinate difference between adjacant lines is Δh_i; in this case, the apparent line spacing would be $w + d_i$. Far away from the indentation and the flowing liquid mound, the surface should be essentially flat and this region provides the reference values for w. Relative to this straight reference line, a set of values of d_i gives the shape of a vertical section through the liquid. The actual values Δh_i are easily calculated. The specific relationships, from Figure 2, are

$$\sin\theta_v = \frac{w}{y_T} \qquad \cos\theta_v = \frac{d_i}{\Delta h_i}\ . \tag{10a,b}$$

A representative experimental picture, showing the distorted rulings, is in Figure 3. The height of the picture is 1·43 cm and the picture width is 0·74 cm. The corresponding actual width on the substrate, as calculated using $\sin\theta_v$, is 1·03 cm. Because the picture size is limited, the moving liquid mound eventually moves out of the field of view. The horizontal white line in the picture indicates the location of the top of the indentation.

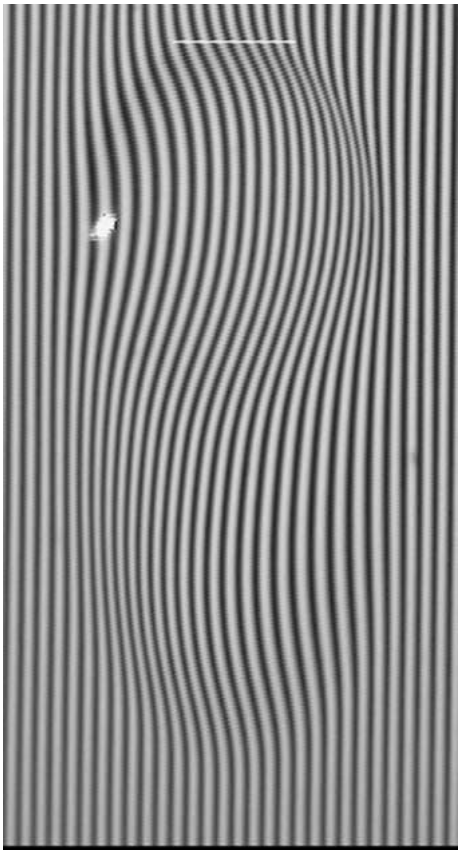

Figure 3. Experimental picture of a distorted pattern of vertical lines on a nonuniform liquid surface; paint IL at 15 seconds after the start of the motion. Each distorted line, after corrections and scaling, is a cross section through the depth of the coating.

It is clear, from an examination of Figure 3, that the stripes can yield the surface shape. Certain corrections need to be applied in order to extract accurate liquid surface shapes from the distorted stripe patterns, however. The most important of these corrects for the deviation of the reference lines from the true vertical. This angular error, which is visible on the vertical sides of Figure 3, is less than 0·5 degree. Yet, because the coating height is a difference measurement, failure to correct for this misalignment causes relatively large error. Another necessary correction is for parallax. As may be seen in Figure 1, the distance from the camera to the lines is not constant. Thus the reference lines are not exactly equally spaced and this must be accounted for. It was found to be more accurate, therefore, to measure the deviation of each line relative to its own ordinate location away from the region of surface deformation.

A more complete discussion of experimental procedures may be found in a companion paper that has recently been submitted [24].

4. Theoretical and experimental results

Figure 4 shows the measured variation in viscosity, in poise, with shear stress, in dynes/cm^2, for the two paints. Using the numerical solution, we determined that the maximum stress, occurring anywhere in the flow, was less than about 500 dyn/cm^2 for the coating thickness

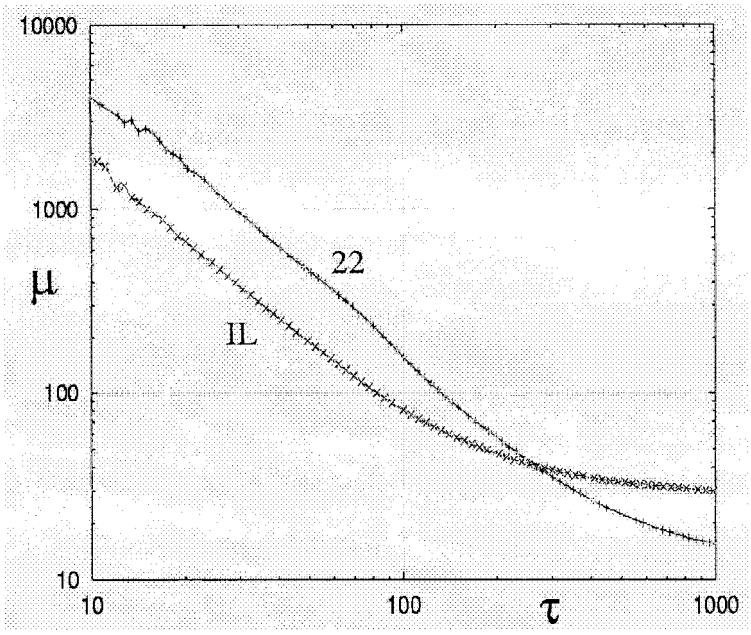

Figure 4. Measured viscosity μ in poise versus shear stress τ in dynes/cm^2 for the two paints used in this study, termed Paint IL and Paint 22.

used in these experiments, Thus the figure includes the entire stress range of interest. This information may be re-plotted in dimensionless form. The viscosity ratio μ_0/μ is plotted versus the shear stress ratio in Figure 5 for paint IL. This ratio, called V in the figure, is seen to be an approximation to the true 'fluidity factor' F that appears in Equation (7). F is calculated from V using the procedure given in the Appendix. It turns out that the fluidity can vary by as much as a factor of 10 or more between different locations in the flow, at a given time. For example, the value of F near the indentation can become large since the liquid depth, and the corresponding stress, can be quite large there. In this sense, these coating liquids are strongly shear thinning.

The experimentally measured surface shapes are compared with the predictions of the theory in Figures 6 and 7. Note that the experimental 'window' size is relatively small and thus paint IL has flowed past the bottom of the window at 30 seconds. A comparison of centerline profiles for the two paints, at two times, in given in Figure 6. The figure shows that the coating flows out of the indentation more readily in the simulation than it does in the experiment. The deviation is greater for paint 22 than for paint IL. Overall the agreement between theory and experiment is remarkably good, at least for paint IL as shown in the upper part of the figure. The shapes of the coating surface in the indentation are in good agreement. The theory predicts that the coating quickly becomes very thin near the upper end of the hole; this is indeed what is observed.

Figure 7 compares contour shapes for the surface of paint IL at the two times. Substrate coordinates are given in units of R, the indentation radius. Values of coating height h are measured in units of h_0. Since h/h_0 oscillates around unity away from the region of interest, in order to avoid confusion, this contour level has been omitted from both the theoretical and the experimentally-derived contour plots. There is, we believe, an impressive degree of similarity between the two sets of plots. The contour levels are the same in the theory and

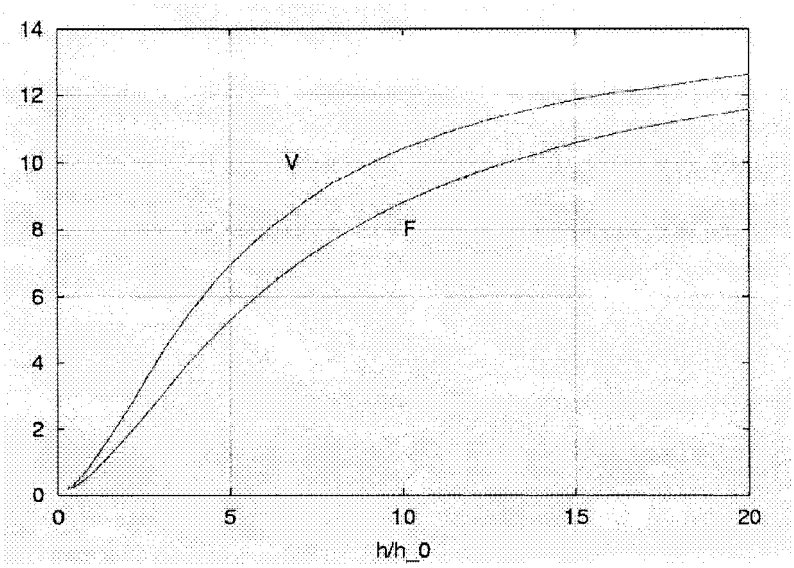

Figure 5. The viscosity ratio $V = \mu_0/\mu$ and the fluidity factor F plotted versus h/h_0 for Paint IL. The variable h/h_0 is equivalent to the stress ratio τ/τ_0 for gravity drainage down a plane vertical wall.

the experimental plots; their values are given in the figure legends. Apart from the fact that the theory predicts slightly greater emptying flow at 15 seconds than is actually observed, the shapes and locations of the depression over the hole and the flowing mound are virtually the same. The experimental profiles also show a high degree of bilateral symmetry.

The slight angularity or jaggedness in the experimental contours is because these plots were constructed using only a total of 300 h values that were distributed uniformly on a 15 by 20 (x, y) grid. Specifically, every second line was used from Figure 3 and the other experimental pictures, yielding a total of 15 lines. The coordinates of twenty equally-spaced points were recorded for each line. The raw data for each point was a pair of pixel coordinates taken from an enlarged version of Figure 3 on a computer monitor. Pixel values are necessarily integers which introduces some small additional error. The experimental surface profiles were subjected to slight smoothing through use of the following 'diffusive' algorithm.

$$h_{ij}^{(k+1)} \leftarrow h_{ij}^{(k)} + \epsilon \left[h_{i+1,j}^{(k)} + h_{i-1,j}^{(k)} + h_{i,j+1}^{(k)} + h_{i,j-1}^{(k)} - 4\, h_{i,j}^{(k)} \right] \tag{11}$$

where ϵ is a number of order 10^{-4}. This is recognizable as the simple explicit finite-difference algorithm that may be used to solve the heat equation. The arrow in (11) signifies replacement. The replacement is performed for all (i, j) interior points and the process is repeated about 100 times. This type of diffusive smoothing is very effective for removing the short-wavelength grid-scale oscillations. In all cases it was verified that the maximum and minimum values of h_{ij} were changed by less than one per cent due to iterative application of (11).

Further comparison between theory and experiment is given in Figure 8. For paint IL, rendered theoretical profiles are shown at 15, 30 and 45 seconds after the start of the motion. Also shown is the 30-second profile, from the experiment, that was photographed using a close-up lens and low-angle lighting. Its appearance is quite similar to the theoretical profile. While rendered pictures do not give quantitative information about the drops, they are more effective for illustratating qualitative features.

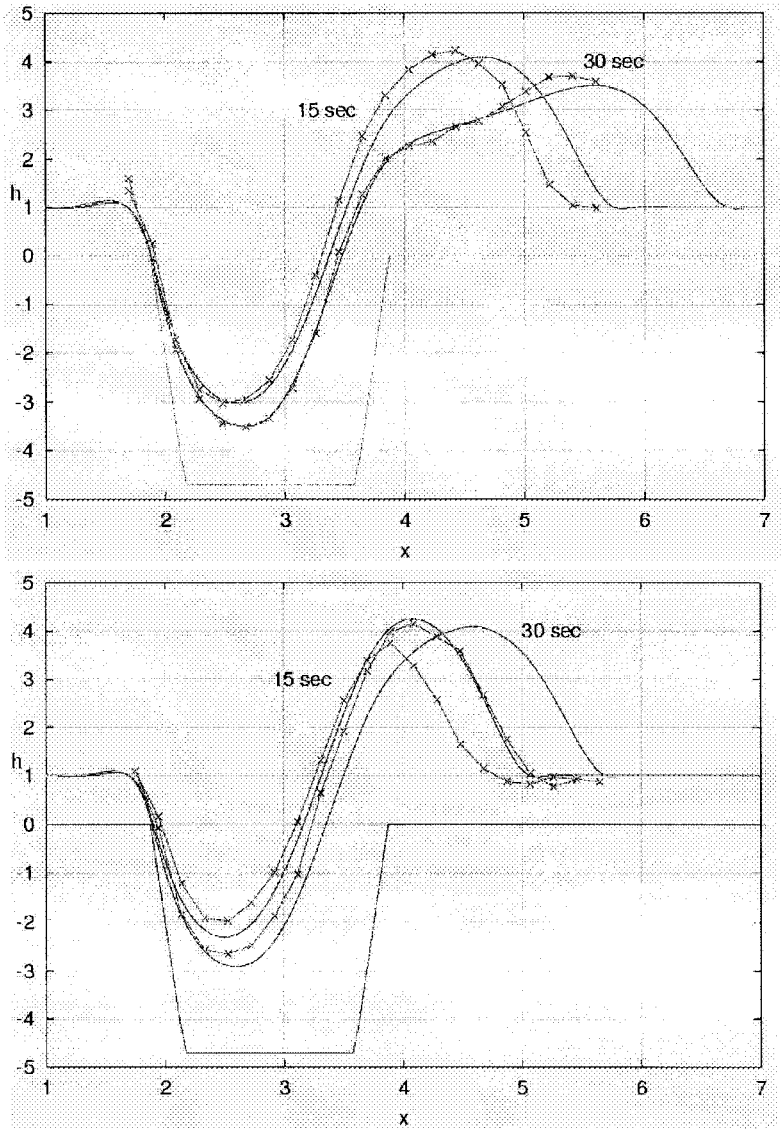

Figure 6. Centerline profiles at two times for the two different coatings; a comparison between experiment and theory. (top) Paint IL; (bottom) Paint 22. The theoretical predictions are shown as solid curves while the experimental results use lines with points. The experimental profiles are derived from ruled photographs, such as that of Figure 3, as explained in the text. The substrate and its indentation are shown using dashed lines. Note that the coating thickness is measured in units of initial thickness h_0 while the substrate length unit is R, the indentation radius.

Various features seen in the simulation are also observed in the experiment. Note the pronounced edge ridge above the indentation. This ridge develops quickly. Its occurrence is readily explained. Surface tension causes the pressure at the edge, where the indentation meets the 'land', to increase. Because this edge is relatively sharp, the pressure becomes large there and it drives the liquid away. The coating thickness, at the edge, becomes quite small, essentially preventing further flow into the indentation from above. The draining liquid 'piles up' above the edge, but also finds a path downward by following the indentation edge. The

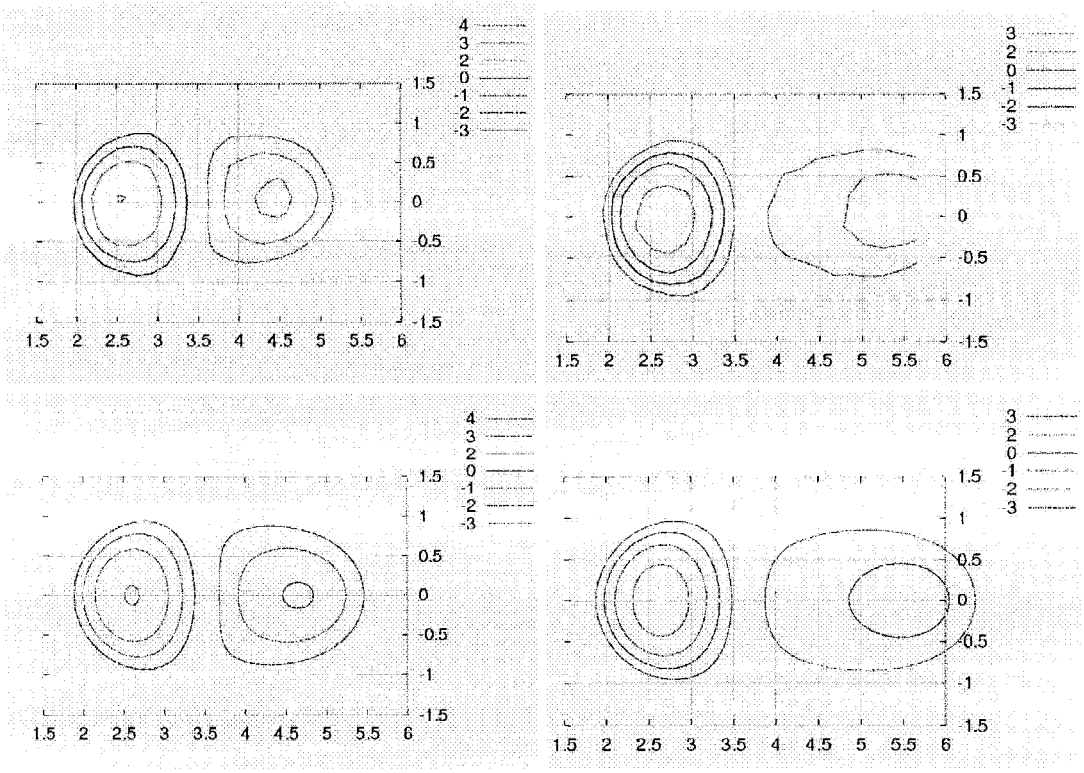

Figure 7. Contour plots of flow out of indentation for Paint IL. Comparison of experimental measurement (top row) with theory (bottom row) Times are 15 seconds (left) and 30 seconds (right).

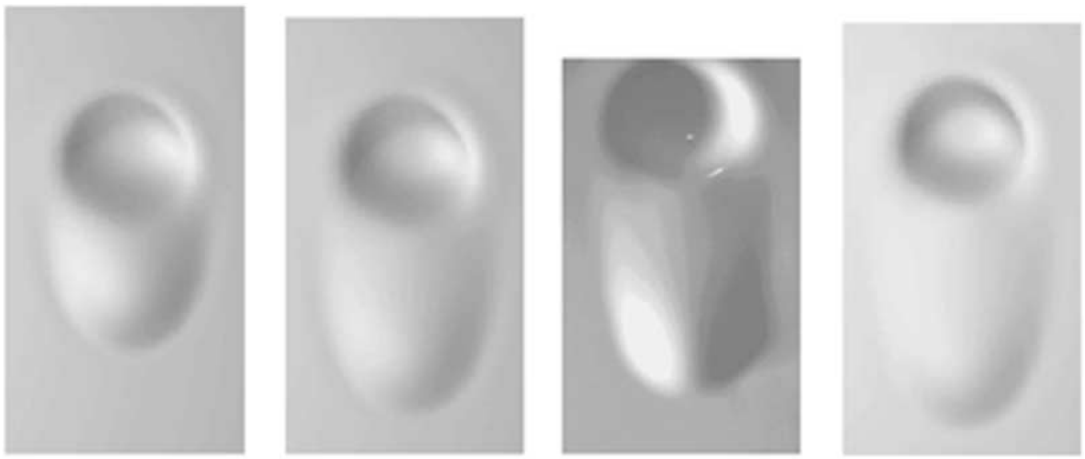

Figure 8. Theoretical and experimental pictures of the draining drop for Paint IL. Three pictures, at times 15, 30 and 45 seconds, are rendered pictures constructed from the theoretical solution. One picture, taken at 30 seconds, is an actual photograph from the experiment.

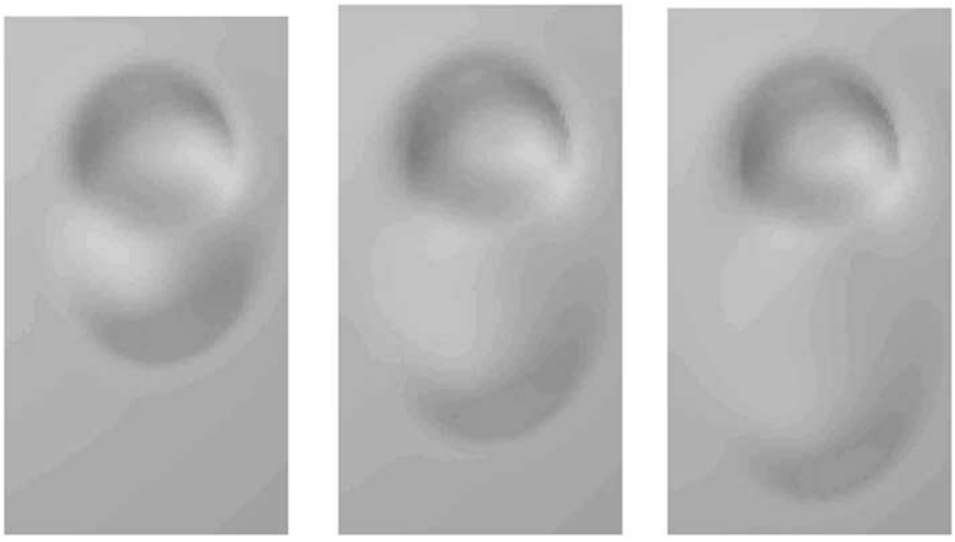

Figure 9. Results of a flow calculation for a Newtonian coating. These pictures can be compared with the shear-thinning paint shown in Figure 8. The Newtonian viscosity is taken to be 135 poise in order to match the length of the drip pattern at 45 seconds.

result is a ridge or ring around the indentation that is easily seen in Figure 8. This behavior is generally undesirable. In decorative-painting applications, the ring will be likely to emphasize an already unsightly defect.

The flow in Figure 8 may be compared with frames from a simulation for a Newtonian paint. Three such frames are shown in Figure 9. The viscosity is arbitrarily selected to be 135 Poise and is constant throughout the flow field. It does not vary with time. The particular viscosity value was selected so that, at 45 seconds, the drainage mound would be similar in length to that shown in Figure 8. Note that, according to the flow model used here, the viscosity only appears in the characteristic time scale T_1^* defined in Equation (8b). Thus, for a Newtonian liquid of constant viscosity, there is only one unsteady solution for a given substrate shape and initial coating thickness. The time to reach any particular subsequent fluid configuration is simply proportional to the viscosity. While the Newtonian drip also slows down as it becomes longer, the slowdown is much more pronounced for shear-thinning liquids. Comparing drip lengths in Figures 8 and 9, one sees that the length difference between 30 and 45 seconds is much larger for the Newtonian liquid. For the shear-thinning liquid, the average viscosity increases substantially since, as the drip becomes longer and less thick, the stress level also decreases. Note also that the shape of the drips is somewhat different. The shear thinning drip is narrower than the Newtonian one because it can only flow easily out of the lowest portion of the indentation where the stress level is high.

Results of theoretical calculations of flow from a wide indentation are shown in Figure 10. Here the indentation diameter is three times the value that was actually used in the experiments. The indentation depth is the same as in the previous cases and the indentation side wall slope is still 45 degrees. The profiles are seen to be quite pointed. This is because surface tension, gravity and the land coating thickness h_0 form the length scale L_1 given in (8a), where L_1 is the scale of small features in the flow field. The ratio of this length scale to the indentation

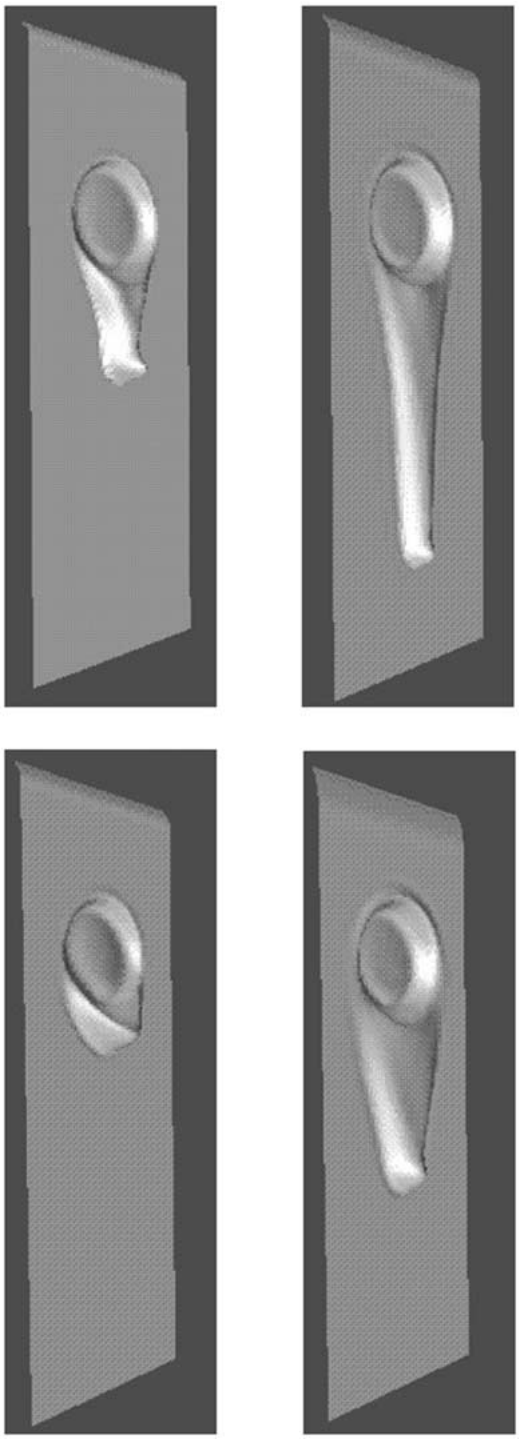

Figure 10. Simulation of flow out of a wider indentation. The diameter here is 2·14 cm which is three times the diameter of the cases treated above. A shear-thinning paint (Paint 22, top row) and a Newtonian paint (100 poise, bottom row) are compared.

radius R determines the general shape of the flow pattern. Thus flows out of small holes will tend to be straight-sided while wide holes will produce drips that are almost wedge-shaped.

The figure also compares the shear-thinning Paint 22 with a Newtonian paint whose viscosity is arbitrarily chosen to be 100 poise. Surface shapes are given at the same two times for each paint. Recall that, for the small indentation previously used, a Newtonian paint with a viscosity of 135 poise emptied at about the same rate as Paint IL. Thus, the 135 poise paint emptied significantly faster than Paint 22 out of the small hole. With the large hole, on the other hand, Paint 22 is faster than a Newtonian liquid of even lower viscosity. This may at first seem puzzling, but it can be easily explained. Because the hole is large, the paint drains to the lower part of the hole as it emerges. The larger volume available for drainage means that the emerging stream will be thick; hence the shear stress becomes quite large. The shear-thinning paint will thus have a low effective viscosity near the dripmark centerline and will drain rapidly there. Note also that the dripmark for Paint 22 takes on a characteristic shape. It is 'hollow ground', *i.e.* concave out. For the Newtonian paint, the drip is more triangular. For Paint 22, there is greater inward flow towards the centerline. This flow replenishes the liquid that is rapidly draining downward. The inward flow is driven by a capillary pressure difference.

5. Concluding remarks

A numerical model, based on the lubrication approximation, has been developed to simulate the three-dimensional time-dependent coating flow of generalized Newtonian liquids. Model results have been validated by comparison with experimental observation. Gravitational emptying of a nail head indentation on a vertical wall was chosen to be the flow problem because of its industrial relevance.

In the course of this work, what we believe to be a new method for measuring the shape of opaque liquid coating layers has been developed. It is simple to implement and requires only that an accurate set of parallel lines be projected onto the liquid surface. The videotape showing the line distortions, when the undulating surface is photographed obliquely, is then subjected to a straightforward analysis to extract a square array of surface ordinates. The results presented here seem to be quite accurate. The method can no doubt be improved further by a systematic re-design. The standard method for extracting the shape of thin liquid layers, interferometry, is most useful for transparent liquids, although an extension to opaque liquids has been reported [25]. In any event, because the basic unit of measurement in interferometry is the wavelength of light, that method is really suitable only for very thin liquid layers. The new method appears to work well for much thicker layers, such as the millimeter-scale layers encountered in this work.

A technique is given in the Appendix that allows the direct utilization of measured rheology data. It has been standard practice to fit rheology data to one of several different functional forms. There is an inevitable loss of accuracy in this process since the standard models are purely empirical and there is no reason why real data should be well-fit by any one of them. If the ultimate use of these data is further computational analysis, and if the particular application is coating flow, the Appendix shows that the data can be used directly without any intermediate fitting step. It is seen to be a straightforward process to convert the measured viscosity curve to an equivalent 'fluidity' function.

The low-speed, long-wavelength, thin-layer, free-surface Newtonian flow theory, commonly referred to as lubrication theory, has been extended to consider liquids whose viscosity is an arbitrary input function of the local shear stress. This theoretical model is solved efficiently on a computer using finite differences and a modified alternating-direction-implicit method. Virtually all features of the observed flow appear to be reproduced by the computation. The good agreement between theory and observation, as in the contour plot comparisons shown in Figure 7, supports the validity of both the data-acquisition (surface imaging) technique and the relatively simple theoretical model.

Further theoretical calculations were made to help explain how the size of geometric features affects the resulting flow patterns. Much larger indentations lead to flows that are qualitatively different; these differences can be adequately explained using the model. There are also characteristic differences between the draining flows of Newtonian and shear-thinning liquids, as shown in Figure 10. This difference in flow shapes is sufficiently pronounced that, after suitable calibration, the shape of a draining 'finger' may itself become useful as a rheological measurement.

For one of the two paints tested, called Paint IL, the agreement between theory and experiment must be considered very good. Considering that the viscosity varies, in space and time, by about two orders of magnitude during a given run, the slight overprediction of emptying rate, at early times, seems quite acceptable. For Paint 22, on the other hand, the speed overprediction is more serious. In Figure 6 one observes that the 30-second experimental profile appears to agree with the theorical 15-second profile. A possible explanation for the lack of better agreement is *thixotropy*, which is a common property of architectural coatings. The hallmark of thixotropy is a dependence of viscosity on the previous stress or strain history of the moving fluid elements. Large prior stress is correlated with lower current values of viscosity. The drawdown blade that is used to apply the uniform initial coating exerts a relatively large shear stress on the coating. This applied stress is nonuniform however, and is smaller for the liquid in the indentation. Thus, the liquid initially within the indentation has not been subjected to the same lowering of viscosity. This may explain the observation of slow initial emptying. General background information on thixotropy and its influences on coating-flow behavior may be found in a recent survey article [26]. Incorporation of thixotropy into an improved draining-flow model is considered to be a high priority task. Models of simple flows, that arise in the coating and food process industries, and that include thixotropy, have been reported [27, 28]. It is also possible, as least in principle, to consider a wider class of viscoelastic flows.

Acknowledgment

The work of LWS was supported by the ICI Strategic Research Fund and the NASA Microgravity Program.

Appendix: The fluidity magnification factor in shear-thinning flow

This Appendix considers the modified fluidity, compared with the flow of a liquid of constant viscosity, that is due to shear-stress-dependent viscosity. A methodology is derived whereby arbitrary generalized Newtonian results, as measured in a viscometer, may be used directly in a numerical procedure, without the need to fit these data to a particular rheology model. The

generalized Newtonian fluid is one for which the viscosity depends solely on the local value of the shear stress. It is found that, when inertia is neglected, all relevant information may be incorporated into a single scalar factor that is an integral function of the viscometer data.

Virtually all coatings of interest are shear-thinning; that is, the viscosity μ decreases as the shear stress τ increases. The particular function $\mu = f(\tau)$ is usually determined experimentally in a viscometer. Typically, the flow in the instrument is *viscometric*, meaning that the strain rate $\dot{\gamma}$ is the same scalar constant throughout the liquid at a given value of imposed stress. Then, in scalar form,

$$\tau = \mu\dot{\gamma} = f(\tau)\dot{\gamma} \ . \tag{A.1}$$

For industrial coatings, f is typically a monotonically decreasing function of its argument.

Let us consider almost-parallel flow of a thin liquid layer, down an almost-flat vertical wall. The local value of total liquid layer thickness is $H(x, y, t)$. The flow is driven by gravity and also by gradients in the capillary pressure $p = -\sigma\kappa$, where κ is the curvature of the liquid free surface. Measure the coordinate z inward from the free surface, so that the substrate corresponds to $z = H$. For small surface inclination, the surface shear stress is a vector with components in the downward x direction and transverse y direction. $\vec{\tau} = \vec{0}$ on the free surface while the drainage speed $\vec{V} = (u, v)$ is virtually parallel to the substrate and is equal to zero there.

For inertialess, or creeping, motion, the sum of the forces on an element of the liquid coating must equal zero. A force balance on an infinitesimal volume element within the liquid readily yields

$$\frac{\mathrm{d}\vec{\tau}}{\mathrm{d}z} = \rho g\,\vec{i} - \nabla p \equiv \vec{k}(x, y) \tag{A.2}$$

where $\vec{i}$ is a unit vector in the downward or x direction. Thus $\vec{\tau} = \vec{k}z$ and the strain rate is essentially

$$\frac{\mathrm{d}\vec{V}}{\mathrm{d}z} = -\frac{\vec{\tau}}{f(\tau)}. \tag{A.3}$$

where τ is the magnitude of $\vec{\tau}$.

The flux $\vec{Q}$ is given by

$$\vec{Q} = \int_0^H \vec{V}\,\mathrm{d}z = \vec{V}z\,|_0^H - \int_0^H z\,\frac{\mathrm{d}\vec{V}}{\mathrm{d}z}\,\mathrm{d}z$$

and the first term on the right is zero, using the boundary conditions. Thus

$$\vec{Q} = \int_0^H z\,\frac{\vec{\tau}}{f(\tau)}\,\mathrm{d}z = \vec{k}\int_0^H \frac{z^2}{f(\tau)}\,\mathrm{d}z \ . \tag{A.4}$$

We wish to compare this flux with that of a reference Newtonian liquid so as to account for the additional flow due to shear thinning. Let

$$F = \left|\frac{\vec{Q}}{\vec{Q}_{\mathrm{ref}}}\right| \ . \tag{A.5}$$

Here $\vec{Q}_{\mathrm{ref}}$ is the flux of the constant-viscosity Newtonian liquid , due to the same force per unit volume $\vec{k}$. The reference viscosity μ_0 is taken to correspond to the stress $\rho g h_0$ where h_0 is the thickness of the initial uniform coating layer. Thus

$$\vec{Q}_{\text{ref}} = \vec{k}\,\frac{H^3}{3f(\rho g h_0)} \tag{A.6}$$

and

$$F = \frac{3f(\rho g h_0)}{H^3}\int_0^H \frac{z^2}{f(kz)}\,\mathrm{d}z\ . \tag{A.7}$$

Here $k = |\vec{k}|$.

Any given plot of viscosity μ versus stress τ may be re-scaled and put into the dimensionless form

$$\frac{\mu}{\mu_0} = R\left(\frac{\tau}{\tau_0}\right) \tag{A.8}$$

where $\tau_0 = \rho g h_0$. Thus $R(1) = 1$. If k were simply equal to ρg, the argument of R would simply be the local layer thickness, ζ say, divided by the reference depth h_0. Because this is not true in general, we will scale the integration variable z in (A.7). Let $z = a\zeta$, then

$$F = \frac{3f(\rho g h_0)}{(H/a)^3}\int_0^{H/a} \frac{\zeta^2}{f(ka\zeta)}\,\mathrm{d}\zeta\ .$$

Now take $a = \rho g/k$; then we have

$$F = \frac{3}{[kH/(\rho g)]^3}\int_0^{kH/(\rho g)} \zeta^2\,\frac{f(\rho g h_0)}{f(\rho g\zeta)}\,\mathrm{d}\zeta = \frac{3}{[kh/(\rho g)]^3}\int_0^{kH/(\rho g)} \frac{\zeta^2}{R(\zeta/h_0)}\,\mathrm{d}\zeta$$

Thus F, the fluidity magnification factor due to shear thinning, is seen to be a function only of the effective depth h_e,

$$F(h_e) = \frac{3}{h_e^3}\int_0^{h_e} \frac{\zeta^2}{R(\zeta/h_0)}\,\mathrm{d}\zeta\ . \tag{A.9}$$

The effective liquid depth is given by

$$h_e = \frac{k}{\rho g}\,H = \frac{k}{\rho g}\,(h - h_1) \tag{A.10}$$

where we recognize that $h(x, y, t)$ and $h_1(x, y)$ are the equations for the moving free surface and the indented substrate, respectively. The zero level for each of the two surfaces is the flat or 'land' area of the substrate. Note that the effective depth includes the weight-increase factor $k/\rho g$. For typical cases considered here, the quantity $h - h_1$ can become as large as eight to ten times the coating thickness h_0 at certain locations and times during the emptying flow. The factor $k/\rho g$ is typically 1·5 or smaller.

Figure 5 shows the factor F and the inverse viscosity ratio $V = \mu_0/\mu$ plotted as a function of stress ratio τ/τ_0. The stress ratio is equivalent to the coating thickness ratio H/h_0 for a perfectly planar free surface. The plot uses the rheology data for paint IL. Note that V is a crude approximation to F. However, F is always less than V because the layer-averaged stress is always less than the stress at the substrate.

References

1. V.G. Levich, *Physiochemical Hydrodynamics*. Englewood Cliffs: Prentice-Hall (1962) 700 pp.

2. J.R.A. Pearson, The instability of uniform viscous flow under rollers and spreaders. *J. Fluid Mech.* 7 (1959) 481–500.
3. S.E. Orchard, Surface levelling in viscous liquids and gels. *Appl. Sci. Res.* 11 (1962) 451–464.
4. J.A. Tallmadge, Withdrawal of flat plates from power law fluids. *AIChE J.* 16 (1970) 925–930.
5. D.E. Weidner and L.W. Schwartz, Contact-line motion of shear-thinning liquids. *Phys. Fluids* 6 (1994) 3535–3538.
6. L.W. Schwartz, Viscous flows down an inclined plane: instability and finger formation. *Phys. Fluids A* 1 (1989) 443–445.
7. L.H. Tanner, Les gouttes (the drops). *La Recherche* 17 (1986) 183–191.
8. L.W. Schwartz and R.R. Eley, Simulation of droplet motion on low-energy and heterogeneous surfaces. *J. Colloid Interf. Sci.* 202 (1998) 173–188.
9. L.W. Schwartz, Hysteretic effects in droplet motions on heterogeneous substrates. *Langmuir* 14 (1998) 3440–3453.
10. A. Sharma and R. Khanna, Pattern formation in unstable thin liquid films under the influence of antagonistic short- and long-range forces. *J. Chem. Phys.* 110 (1999) 4929–4936.
11. L.W. Schwartz, R.V. Roy, R.R. Eley and S. Petrash, De-wetting patterns in a drying liquid film. *J. Colloid Interf. Sci.* 234 (2001) 363–374.
12. D. Peaceman, *Fundamentals of Numerical Reservoir Simulation*. Amsterdam: Elsevier North-Holland, (1977) 176 pp.
13. M.H. Eres, L.W. Schwartz and R.V. Roy, Fingering phenomena for driven coating films. *Phys. Fluids* 12 (2000) 1278–1295.
14. M.A. Spaid and G.M. Homsy, Stability of Newtonian and viscoelastic dynamic contact lines. *Phys. Fluids* 8 (1996) 460–478.
15. D.E. Kataoka and S.M. Troian, A theoretical study of instabilities at the advancing front of thermally driven coating films. *J. Colloid Interf. Sci.* 192 (1997) 350–362.
16. P.G. Lopez, M.J. Miksis and S.G. Bankoff, Stability and evolution of a dry spot. *Phys. Fluids* 13 (2001) 1601–1614.
17. D.J. Benney, Long waves on liquid films. *J. Math. Phys.* 45 (1966) 150–155.
18. R.W. Atherton and G.M. Homsy, On the derivation of evolution equations for interfacial waves. *Chem. Eng. Comm.* 2 (1976) 57–77.
19. A. Oron, S.H. Davis and S.G. Bankoff, Long-scale evolution of thin liquid films. *Rev. Mod. Phys.* 69 (1997) 931–980.
20. R.B. Bird, R.C. Armstrong and O. Hassager, *Dynamics of Polymeric Liquids*. New York: Wiley (1977) 470 pp.
21. J.S. Kim, S. Kim and F. Ma, Topographic effect of surface roughness on thin-film flow. *J. Appl. Phys.* 73 (1993) 422–428.
22. S. Kalliadasis and G.M. Homsy, Stability of free-surface thin-film flows over topography. *J. Fluid Mech.* 448 (2001) 387–410.
23. L.W. Schwartz, P. Moussalli, P. Campbell and R.R. Eley, Numerical modeling of liquid withdrawal from gravure cavities in coating operations. *Trans. Inst. Chem. Engrs.* 76 (1998) 22–29.
24. R.R. Eley and L.W. Schwartz, Interaction of rheology, geometry, and process in coating flows. *J. Coatings Technol.* (2001) submitted.
25. M. Klarskov, J. Jakobsen and A. Saarnak, Verification of the Orchard leveling analysis. *Rheology* 92 (1992) 30–39.
26. R.R. Eley, Rheology in coatings, principles and methods. In: R.A. Meyers (ed.), *Encyclopedia of Analytical Chemistry*. Chichester: Wiley, Chichester (2000) pp. 1839–1869.
27. O. Cohu and A. Magnin, The levelling of thixotropic coatings. *Prog. Organic Coatings* 28 (1996) 89–96.
28. C. Baravian and D. Quemada, Modelling thixotropy using a novel structural kinetics approach: basis and application to a solution of iota carrageenan. *J. Texture Studies* 27 (1996) 371–390.